Check for updates

ADVANCED MATERIALS
www.advmat.de

Bio-Inspired Pressure-Dependent Programmable Mechanical Metamaterial with Self-Sealing Ability

Naeim Ghavidelnia, Viacheslav Slesarenko, Olga Speck, and Christoph Eberl*

Self-sealing is one of the fascinating functions in nature that enables living material systems to respond immediately to damage. A prime plant model is *Delosperma cooperi*, which can rapidly self-seal damaged succulent leaves by systematically deforming until the wound closes. Inspired by this self-sealing principle, a novel programmable mechanical metamaterial has been developed to mimic the underlying damage management concept. This material is able to react autonomously to changes in its physical condition caused by an induced damage. To design this ability into the programmable metamaterial, a permeable unit cell design has been developed that can change size depending on the internal pressure. The parameter space and associated mechanical functionality of the unit cell design is simulated and analyzed under periodic boundary conditions and various pressures. The principles of self-sealing behavior in designed metamaterials are investigated, crack closure efficiency is identified for different crack lengths, the limitations of the proposed approach are discussed, and successful crack closure is experimentally demonstrated in the fabricated metamaterial. Although this study facilitates the first step on the way of integrating new bio-inspired principles in the metamaterials, the results show how programmable mechanical metamaterials might extend materials design space from pure properties to life-like abilities.

1. Introduction

For many years, scientists have striven to create engineered materials with the built-in ability to automatically repair themselves without external diagnosis or human intervention. Several studies[1,2] have shown that the self-repair process of biological and artificial material systems, including bio-inspired material systems, can be divided into a rapid self-sealing phase and a subsequent longer-term self-healing phase. As a fundamental premise, the self-repairing process in material models begins with self-sealing, swiftly reinstating the system's "mechanical functionality" by preventing further damage propagation. This initial phase prevents complete system collapse and assists in the realization of the subsequent self-healing phase. The aim of the self-healing phase is to gradually restore the material system's "mechanical properties", such as stiffness and strength. Successful completion of both self-sealing and self-healing phases is essential for the restoration of mechanical properties and load-bearing capacity in the self-repairing process. Nevertheless, artificial materials are generally referred to as self-healing materials.[3–5] The engineered materials designed and established for self-healing purposes to date include all classes of materials, such as polymers or elastomers with embedded internal adhesives that can be activated in response to an external stimulus (light, temperature, etc.) to initiate the healing processes,[6–11] metals with an intrinsic repair mechanism of the material to the addition of a repair agent contained in microscopic vessels,[12–15] ceramic matrix composites having a self-healing mechanism of particle rearrangement or viscous flow of a glass melt into the crack and restoration of material strength,[16–18] and cementitious materials containing capsules of bacterial spores that start the production of $CaCO_3$ crystals when water enters the concrete cracks.[19–21] However, while self-healing materials can self-repair damage by closing microscopic cracks, they do not provide successful healing mechanisms for larger cracks.[22–24] This shortcoming is because conventional self-healing materials rely on the ability to initially flow into the damaged area, and if the crack is too large, the material would not be able to flow into the crack and repair it. In both living and artificial material systems, this phase is called the self-sealing or mobile phase, which

N. Ghavidelnia, V. Slesarenko, O. Speck, C. Eberl
Cluster of Excellence livMatS @ FIT — Freiburg Center for Interactive Materials and Bioinspired Technologies
University of Freiburg
Georges-Köhler-Allee 105, D-79110 Freiburg, Germany
E-mail: naeim.ghavidelnia@livmats.uni-freiburg.de
O. Speck
Plant Biomechanics Group @ Botanic Garden Freiburg
University of Freiburg
Schänzlestr. 1, D-79104 Freiburg, Germany
C. Eberl
Materials Design Department Fraunhofer Institute for Mechanics of Materials (IWM)
Wöhlerstr. 11, D-79108 Freiburg, Germany

The ORCID identification number(s) for the author(s) of this article can be found under https://doi.org/10.1002/adma.202313125

© 2024 The Authors. Advanced Materials published by Wiley-VCH GmbH. This is an open access article under the terms of the Creative Commons Attribution License, which permits use, distribution and reproduction in any medium, provided the original work is properly cited.

DOI: 10.1002/adma.202313125

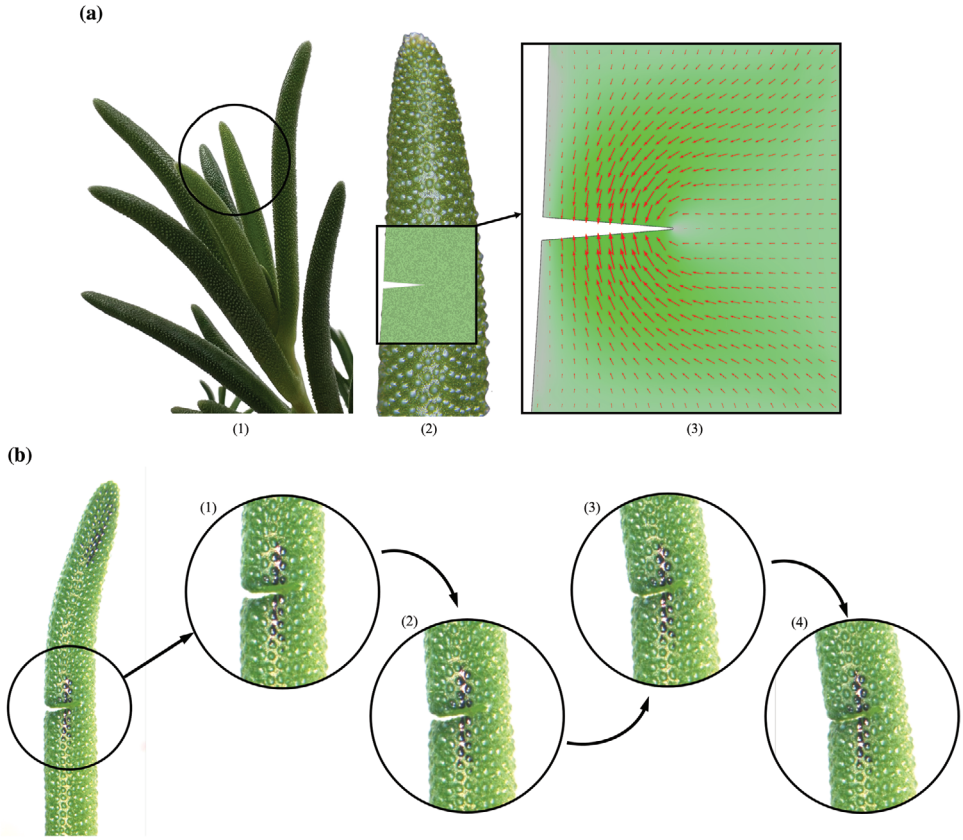


Figure 1. Self-sealing function of the plant model *Delosperma cooperi*. a.1) *Delosperma cooperi* plant with succulent leaves, a.2) schematic drawing of a transverse cut projected onto a leaf, a.3) simulation of water flow to the outside due to the distortion of hydro-mechanical equilibrium, b) self-sealing process of the succulent leaves of *Delosperma cooperi*, b.1) 15 minutes, b.2) 25 minutes, b.3) 37 minutes, b.4) 47 minutes after introducing a transverse cut by a razor blade. Adopted from ref. [29]

refers to the ability of plants, animals, and inanimate material to seal the damage.[1] With self-sealing ability, the material can close larger cracks and gaps, allowing the material to reduce the cracks size and complete the repair process afterward.[25] Therefore, self-sealing is a necessary step before the self-healing process, especially for materials that are prone to larger cracks. The subsequent self-healing step, which involves various chemical reactions and more complex processes, could heal the damage and restore the mechanical performance of the material.

In advanced biomimetic material systems, both self-sealing and self-healing principles have to be implemented.[1] In plants, rapid self-sealing of external wounds, manifested as superficial closure of the injury, prevents dehydration and infection by external germs.[26,27] Additionally, internal growth-related incisions are rapidly closed, preventing the gap from expanding to the surface and eliminating potential entry points for infection.[28] In this study, we specifically investigate the wound-sealing principle of *Delosperma cooperi* as a plant model (**Figure 1**). Following external damage, the succulent leaves of *Delosperma cooperi* exhibit a self-sealing principle through the deformation of the entire leaf, completed in approximately 60 minutes. After transverse (Figure 1b) and longitudinal cuts, the leaves bend, and after a circumferential cut, they contract until the wound edges meet.[29] The self-sealing principle of *Delosperma cooperi* involves a hydrostatically driven deformation of the entire leaf, captured by a numerical model.[30] Furthermore, the deformation can be accelerated through mechanically driven deformation based on alternatively pre-tensioned and pre-compressed tissue layers,[31] a principle substantiated by an analytical model.[32] Immediately after injury, a rapid initial opening in the wound area occurs due to pre-tension in the dermal tissue layer. Subsequent wound closure is primarily a hydrostatically driven deformation, serving as a model for self-sealing principle transferred from biological world to engineering paradigm in the present study. The numerical model,[30] based on the theory of porous flow and poroelasticity, indicates that water loss through the free wound surfaces initiates the self-sealing process. Consequently, the turgor pressure of the parenchyma cells in the wound area decreases, and water loss is compensated by water flow from the surrounding parenchyma. This flow creates a pressure gradient that propels the deformation of the entire leaf, bringing the wound edges into contact and resulting in the self-sealing of the wound (Figure 1b).

Inspired by the mechanically driven self-sealing principle of *Delosperma cooperi* leaves, Yang et al.[33] developed a self-healing polymer. At a temperature of 65°C, an 8 μm × 50 μm scratch is optically healed within 10 minutes. After 120 minutes, mechanical properties (e.g., stress at break, tensile strain) are restored by more than 80%. Becker et al.[34] developed a biomimetic multilayer actuator with self-sealing function. Inspired by the prestresses in the *Delosperma cooperi* leaf, they developed a planar

© 2024 The Authors. Advanced Materials published by Wiley-VCH GmbH

15214095, 2024, 27, Downloaded from https://onlinelibrary.wiley.com/doi/10.1002/adma.202313125 by ALbert-Ludwigs-Universitaet, Wiley Online Library on [20/12/2024]. See the Terms and Conditions (https://onlinelibrary.wiley.com/terms-and-conditions) on Wiley Online Library for rules of use; OA articles are governed by the applicable Creative Commons License

three-layer material system with built-in pre-stresses. Triggered by the damage to one layer, the entire material system bends until the damage edges meet.

To achieve an engineered material capable of self-sealing, it appears that intricate mechanisms and specific features are necessary to effectively replicate natural mechanisms, such as those found in plants. Mechanical metamaterials, with their extreme potential for being designed to exhibit unique mechanical properties[35–37] and functionalities,[38–40] could serve as a distinctive solution for developing new material systems that mimic self-sealing in plants and efficiently close large cracks. In this study, inspired by the *Delosperma cooperi* plant, we propose a novel programmable mechanical metamaterial by implementing hydraulic pressure-dependent unit cells that exhibits the self-sealing function according to the corresponding biological model. We present a comprehensive description of the geometrical design of the unit cells, elucidating the crucial mechanical properties and behaviors necessary for the self-sealing function based on the plant model. The effective parameters of these unit cells are clearly defined and thoroughly investigated. To capture the available design space and the range of mechanical properties for the metamaterial, we conduct a comprehensive set of nonlinear finite element analyses of the single unit cells with various geometrical parameters. In addition to analyzing the elastic properties of the metamaterial, we explore the major fluidic features, such as porosity and permeability, and discuss the influence of these parameters in the self-sealing process. Subsequently, by introducing a crack in the metamaterial, we illustrate the active and successful self-sealing function that leads to an effective closure of the damaged metamaterial. Besides demonstrating feasibility of self-sealing in the developed metamaterial, we study the sealing effectiveness for different crack lengths, noting existing limitations and suggesting available solutions for improvement. Finally, we propose a new method of manufacturing such permeable metamaterials with a large number of unit cells and demonstrate the crack-closure effect for a sample of mechanical metamaterial.

2. Results and Discussion

Inspired by the remarkable self-sealing abilities of the succulent plant *Delosperma cooperi*, our designed mechanical metamaterial exhibits a similar self-sealing capability that enables it to restore functionality after structural damage. A schematic representation of the developed metamaterial, inspired by the self-sealing process of *Delosperma cooperi*, is shown in **Figure 2**. Its primary innovation lies in the pressure-dependent structures of its unit cells, which can expand in response to internal hydrostatic pressures and store mechanical energy for autonomous reactions (Figure 2a). The unit cells of the metamaterial are designed with a permeability feature, facilitating fluid exchange between neighboring cells in case of any disturbance, such as damage, in the mechanical equilibrium of the system. When a crack occurs, the fluid within the material begins to seep out due to the differential pressures inside and outside the material (Figure 2b). This fluid flow, owing to the permeability of the interconnected structure, generates a pressure gradient around the damaged area (Figure 2c), resulting in global deformation in the metamaterial. As a consequence, the metamaterial contracts in the damaged zone and restores its functional integrity by bringing the crack surfaces together (Figure 2d). In the following sections, we explain the details of the different structural features of the designed mechanical metamaterial and discuss the self-sealing ability of this mechanical metamaterial.

Figure 3a illustrates the fundamental design of the unit cell, showcasing the essential features required for self-sealing ability. The primary characteristic necessary for the unit cells of the mechanical metamaterial is a substantial volume change resulting from internal hydraulic pressure. This pressure-dependent volume change is achieved by integrating bending-dominant elements, such as curved shells, into the square-shaped, bending-dominant unit cells. The second vital characteristic that unit cells must fulfill is the permeability of the structure walls. Since the interconnected lattice structure of the corresponding mechanical metamaterial should facilitate the flow of internal fluid from each unit cell to the neighboring cells, a small hole is introduced at the center of each curved shell. The complete geometrical description of the unit cell, including short and long arc lengths, is available in Section SA (Supporting Information). To investigate the pressure dependency of the unit cells under large deformations, finite element analysis is conducted under periodic boundary conditions in horizontal and vertical directions, with internal hydrostatic pressure (P_0) as the loading condition, as depicted in Figure 3b. To capture the realistic geometry change of the unit cell under high strain due to high internal pressure, the hyperelastic nonlinear material model is considered for the base material of the structure. Detailed information about the material model and finite element simulations can be found in Section SB.1 (Supporting Information). The pressure-volume response graph for a specific unit cell with a normalized radius of $r/l = 0.31$ and slenderness ratio of $t/l = 0.075$ is presented in Figure 3c. As anticipated from the curved shells of the structure, a nonlinear pressure-volume behavior is observed, indicating a significant change in the mechanical properties due to volume change. With increasing internal normalized pressure (P/P_{max}), the curved shells begin to flatten, and the total volume of the unit cell increases until the critical region where the stretching stiffness of the shells becomes dominant compared to the bending stiffness. For the depicted configuration in Figure 3c, this transition occurs between 0.3 and 0.4 of the volume change ratio ($\Delta V/V_1$). During this transition, the effective elastic modulus of the unit cell and the corresponding metamaterial structure dramatically increase, resulting in a higher slope ($E_2 > E_1$) of the pressure-volume graph, increasing the elastic stiffness of the metamaterial. At higher pressure values, when the curved shells are fully stretched with almost zero curvature, the stiffness of the structure slightly decreases due to the thickness reduction. The pressure (or volume) dependency of stiffness plays a crucial role in the final design of the metamaterial system with self-sealing ability, which must function in a specific predefined pressure range and respond to pressure changes resulting from damage.

To attain distinct pressure-volume behaviors for the mechanical metamaterial, a fundamental prerequisite for achieving successful crack closure in the self-sealing mechanism for different crack sizes, we propose adjusting the behavior based on two main parameters of the unit cell. **Figure 4**a,b illustrates the effects of various thicknesses and radii of the shells on the pressure-volume behavior of short arc unit cells. Both

© 2024 The Authors. Advanced Materials published by Wiley-VCH GmbH

15214095, 2024, 27, Downloaded from https://onlinelibrary.wiley.com/doi/10.1002/adma.202313125 by Albert-Ludwigs-Universitaet, Wiley Online Library on [20/12/2024]. See the Terms and Conditions (https://onlinelibrary.wiley.com/terms-and-conditions) on Wiley Online Library for rules of use; OA articles are governed by the applicable Creative Commons License

15214095, 2024, 27, Downloaded from https://onlinelibrary.wiley.com/doi/10.1002/adma.202313125 by ALbert-Ludwigs-Universitaet, Wiley Online Library on [20/12/2024]. See the Terms and Conditions (https://onlinelibrary.wiley.com/terms-and-conditions) on Wiley Online Library for rules of use; OA articles are governed by the applicable Creative Commons License

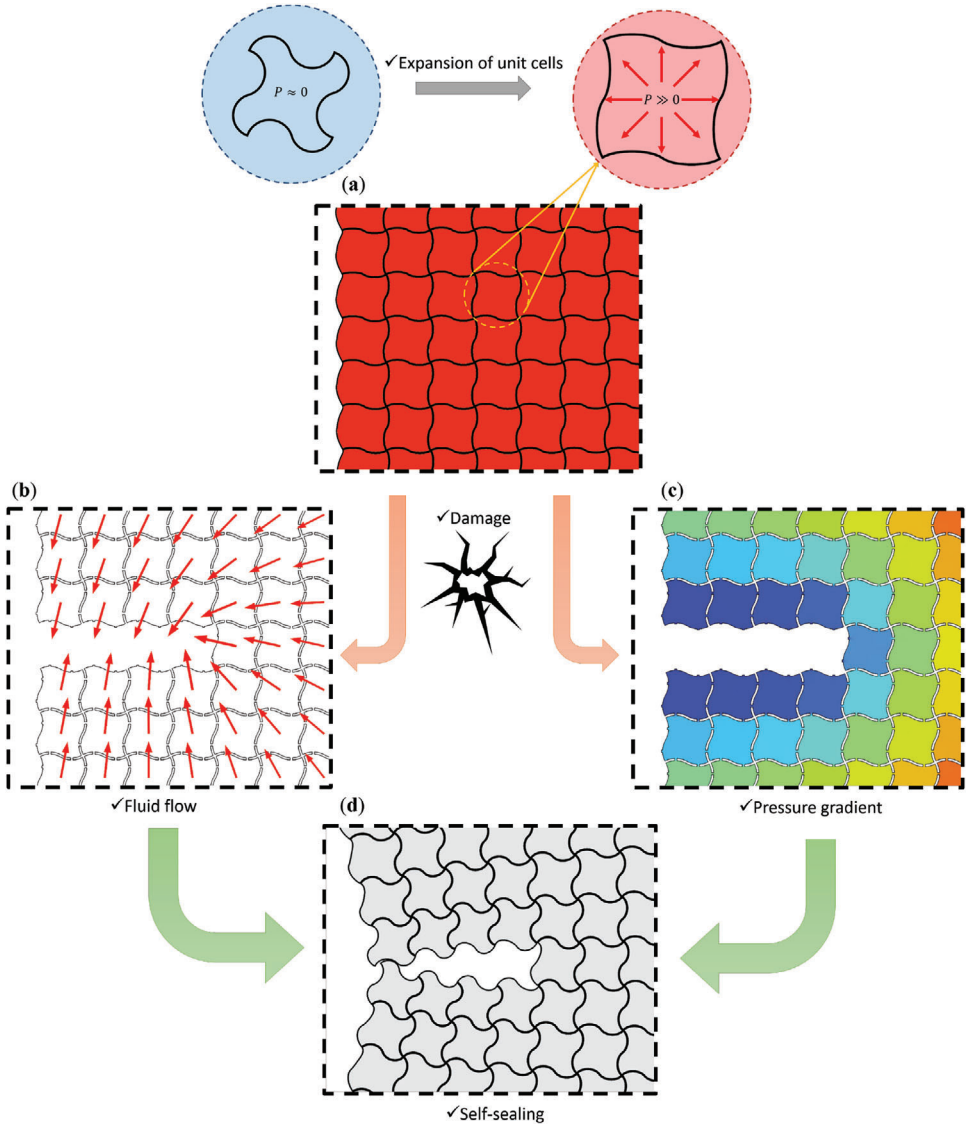


Figure 2. Schematic representation of the self-sealing mechanical metamaterials. a) Higher energy state through pressurizing the unit cells of the intact metamaterial, b) fluid flow to the crack zone triggered by the damage, c) subsequent pressure gradient in the porous media due to fluid flow, d) self-sealing of the crack gap resulted by the metamaterial responds to the new loading condition.

thickness (t) and radius (r) values are normalized with respect to the unit cell length (l) to present the results in a practical manner for upscaling or downscaling. The internal hydrostatic pressure (P) and volume change ($\Delta V = V_2 - V_1$) values are also normalized with respect to the maximum pressure (P_{max}), making the curvature of unit cell shells near zero, and the initial volume (V_1) of the unit cell before pressurizing, respectively. In general, changing the normalized radius has a significant impact on the potential volume change in the unit cell. Smaller radii result in longer shell curves and, consequently, a greater ability for volume change in short arcs unit cells. It is worth noting that the minimum limit of the normalized radius of the shells is restricted to $r/l = 0.25$, leading to an arc with $\theta = 180°$, which yields the highest volume change and lowest stiffness compared to other configurations. Higher volume changes are also achievable for some configurations with long arcs having $\theta > 180°$ (see Section SA, Supporting Information). The transition from bending-dominant curved shells (with low stiffness) to stretching-dominant straight shells (with high stiffness) for all unit cells occurs in the range of 0.1 to 0.2 of the normalized pressure and is smoother for lower values of r/l (Figure 4a). Therefore, by adjusting the normalized radius of the shells (r/l), control over the volume change, the pressure range needed for inflation, and the stiffness of the structure is achievable. On the other hand, Figure 4b demonstrates the adjustment of properties by varying the slenderness ratio of the shells. Increasing the slenderness ratio (t/l) linearizes the pressure-volume behavior and diminishes the effect of stiffness change. Consequently, the stiffness transition region can be fine-tuned by altering the thickness of the shells to achieve the desired properties.

To ensure that the design of a permeable structure has the ability to meet the required permeability and porosity properties

 © 2024 The Authors. Advanced Materials published by Wiley-VCH GmbH

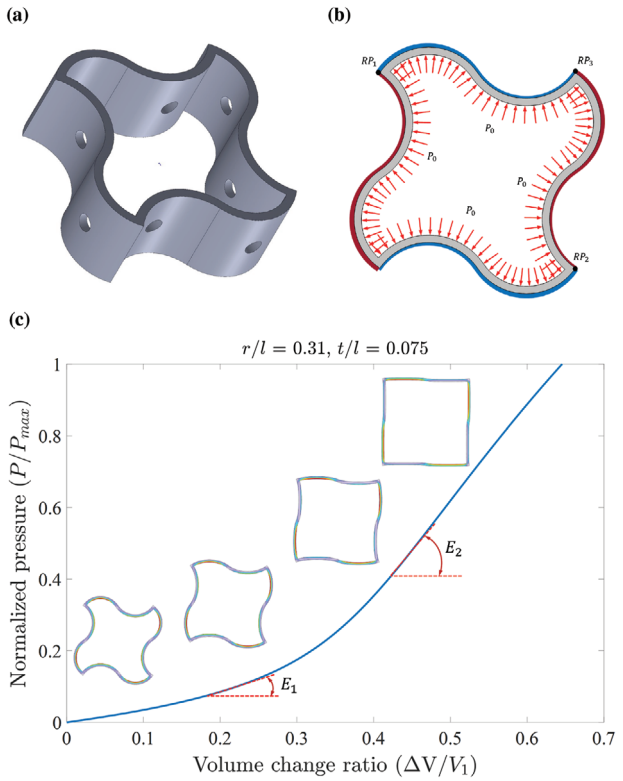


Figure 3. Mechanical behavior of the designed unit cells of the mechanical metamaterial. a) Expandable unit cell shape with internal holes for permeability. b) Periodic boundary conditions with guiding reference points (RP_1, RP_2, and RP_3) in horizontal (red) and vertical (blue) directions and internal pressure (P_0) as loading condition. c) Pressure-volume behavior of unit cells, where the slope of the curve corresponds to the effective elastic modulus E.

for creating the proper flow rate and pressure gradient necessary for a successful sealing mechanism, we conducted a finite element analysis of creep flow for the corresponding mechanical metamaterial (see **Figure 5**). Detailed information about the finite element modeling can be found in Section SB.2 (Supporting Information). Figure 5a illustrates the interconnected fluid cavity of a porous lattice structure composed of 10 by 10 unit cells, where the right-hand side is under high pressure ($P_{in} = P_0$) and the left-hand side is under low pressure ($P_{out} = 0$). Due to the pressure difference on both sides of the interconnected lattice, as per Darcy's law, fluid flow (Q) is generated from the inlet to the outlet of the media, creating a pressure drop for each unit cell that the flow crosses. Consequently, a pressure gradient is established within the porous media of the mechanical metamaterial. Permeability (κ) and porosity (ϕ) are crucial properties influencing fluid flux and pressure gradient within the porous metamaterial. Porosity is the geometrical feature of the metamaterial, defined as the fraction of the volume of voids over the total volume of the structure ($\phi = \frac{V_{void}}{V_{total}}$), dictating the amount of fluid that can be stored in the metamaterial in its intact form. Permeability is the other main property controlling fluid flux and the resistance of the fluid to move through the porous media of the metamaterial. Although the hole diameter plays a negligible role in the porosity of the structure, the thickness of the shells shows a significant impact on the porosity and consequently the fluid storage capacity of the metamaterial. In Figure 5b, the variation of the ratio of permeability of the structure to dynamic viscosity of the fluid ($\frac{\kappa}{\mu}$) is demonstrated. This ratio represents the resistivity of the metamaterial to the movement of the fluid within the interconnected lattice structure. The ratio is dramatically changed by altering the normalized hole diameter in the unit cells from 0.09 to 0.01, reducing the permeability up to six times for the same fluid. It is worth noting that the ratio of permeability over dynamic viscosity explains the speed of the fluid moving out from the metamaterial due to the existing pressure gradient. Hence, the higher the ratio, the faster the metamaterial gets depressurized. The results show that by utilizing different thicknesses and hole diameters, various values of permeability and porosity are achievable, which can be adjusted for different conditions to have fast or slow sealing mechanisms.

Figure 6a illustrates an artificial leaf of *Delosperma cooperi* composed of pressure-dependent unit cells with $r/l = 0.26$ and $t/l = 0.075$ from a mechanical metamaterial, subjected to a transverse crack. The initial condition is characterized by high hydrostatic pressure, generated by the fluid stored in the intact metamaterial structure. Upon the introduction of damage, a pressure difference between the internal fluid and the atmosphere causes the internal stored fluid to flow out of the metamaterial, seeking a new physical equilibrium. Figure 6b illustrates the stabilized physical condition of the internal fluid after the damage occurs in the metamaterial. Boundaries located far from the cracked zone exhibit high pressure values (P_0) due to the surrounding internal pressure. Conversely, boundaries at the crack surface have pressures equal to zero, resulting from the outflow to atmospheric pressure. The pressure gradient, a consequence of fluid flow, varies from P_{max} at the corner of the lattice (i.e., at the maximum distance from the crack) to P_{min} at the surrounding damaged zone of the lattice (i.e., at the crack surfaces). Other unit cells between these boundaries, with varying hydraulic pressures, contribute to a gradient from P_{max} to P_{min} based on their distance from the crack surfaces. Upon subjecting the metamaterial to a crack, as depicted in Figure 6b (with the crack length is considered to be 45% of the total length of the lattice structure), the self-sealing process initiates through the interaction between unit cells by exchanging the fluid and creating a fluid flow towards the cracked area. These cells locally exchange fluid, creating a global pressure gradient within the metamaterial structure. The resultant varied pressures in each unit cell lead to different volumes in corresponding unit cells within the metamaterial lattice. Based on these pressures, the unit cells surrounding the crack surfaces deflate faster than distant unit cells, causing a significant variation in volumes between unit cells. This volume difference induces a shape change in the entire structure, ultimately squeezing and completely closing the crack surfaces (Figure 6c). Details regarding the finite element simulations, detailed loading conditions and procedure of the crack closure modeling can be found in Section SB.1 (Supporting Information). It is essential to note that the slight unsymmetrical deformation of the metamaterial during crack closure is due to the chirality effect of the structure, leading to an asymmetrical fluid flow and, consequently, a pressure gradient, as demonstrated in Section SB.2 (Supporting Information).

© 2024 The Authors. Advanced Materials published by Wiley-VCH GmbH

15214095, 2024, 27, Downloaded from https://onlinelibrary.wiley.com/doi/10.1002/adma.202313125 by Albert-Ludwigs-Universitaet, Wiley Online Library on [20/12/2024]. See the Terms and Conditions (https://onlinelibrary.wiley.com/terms-and-conditions) on Wiley Online Library for rules of use; OA articles are governed by the applicable Creative Commons License

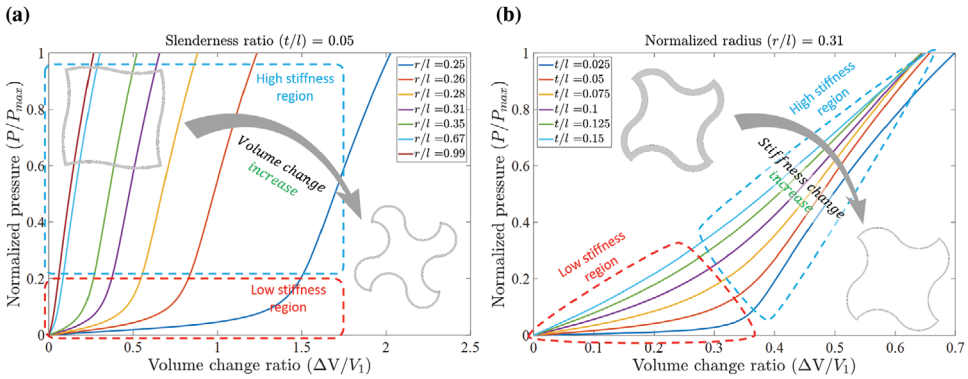


Figure 4. Pressure-volume behavior of the unit cells. a) Effect of normalized radius (r/l) of the shells on the pressure-volume behavior (t/l = *const.*), b) effect of slenderness ratio (t/l) on the pressure-volume behavior (r/l = *const.*).

It must be pointed out that successful crack closure is limited and only possible with some of the available configurations of unit cells, requiring specific normalized radius and slenderness ratio. To gain a deeper understanding of the crack closure limitation, two different configurations for unit cells with $r_1/l = 0.26$ and $r_2/l = 0.28$ are considered (cf. **Figure 7**). As described in Figure 6, the metamaterial made by unit cells with a lower normalized radius ($r_1/l = 0.26$) can close the crack within a specific pressure gradient ranging from $P/P_{max,1} = 0.055$ to $P/P_{min,1} = 0.006$, where $P/P_{min,1}$ and $P/P_{max,1}$ represent the minimum and maximum pressures in the unit cells of the metamaterial after the crack occurs. The corresponding required volume change ratio for this pressure difference is calculated as $\Delta V_1/V_1 = \frac{V_{max,1} - V_{min,1}}{V_1} = 0.477$ (blue line in Figure 7). Therefore, this volume change is necessary for the successful crack closure of the metamaterial. By considering the same required volume change for the metamaterial structure with $r_2/l = 0.28$ (red line in Figure 7), the maximum normalized pressure of $P/P_{max,2} = 0.114$ is calculated. However, since the ratio of the maximum to minimum pressure in the lattice structure must be constant ($\frac{P_{max}}{P_{min}} = const.$) due to the creep flow of the fluid in porous media, the minimum pressure around the cracked area cannot reach the required minimum volume ratio ($\Delta V_2/V_1 = \frac{V_{max,1} - V_{min,1}}{V_1} = 0.365$) to create the necessary volume change ratio for this pressure difference. Therefore, the metamaterial structure with $r_2/l = 0.28$ will not be able to close the crack completely (red structure in Figure 7), whereas the structure with $r_1/l = 0.26$ facilitates the successful crack closure (blue structure in Figure 7). It is also worth noting that due to the higher stiffness (or steeper slope of the pressure-volume graph) of the metamaterial with $r_2/l = 0.28$, choosing a higher pressure of $P/P_{max,2}$ could not improve the sealing efficiency because $P/P_{min,2}$ also increases dramatically.

The crack length is another crucial aspect of sealing efficiency that should be addressed, as it significantly influences successful crack closure and the self-sealing mechanism. To analyze the effect of crack length, the metamaterial lattice was subjected to

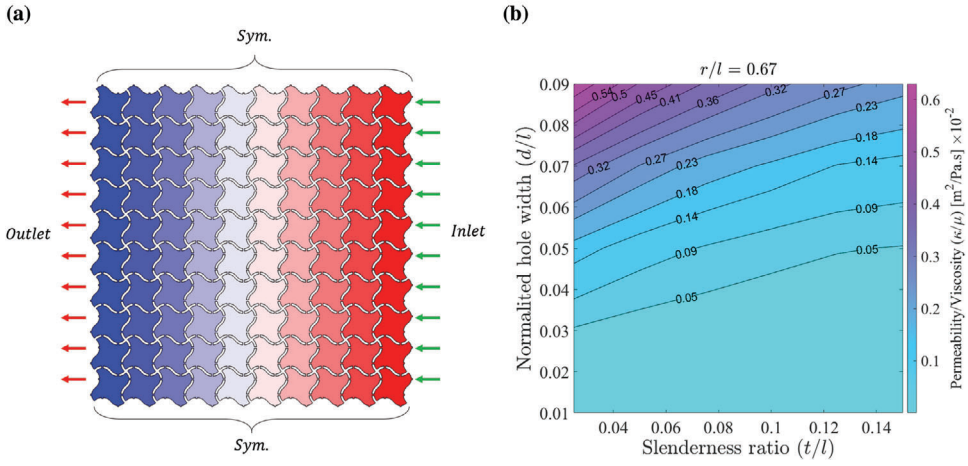


Figure 5. Finite element models of a lattice structure composed of 10 by 10 unit cells. a) The creep flow of the fluid within the interconnected metamaterial structure with symmetrical boundary condition at top and bottom, b) the effect of normalized hole diameter and slenderness ratio on the ratio of permeability over dynamic viscosity ($\frac{\kappa}{\mu}$).

© 2024 The Authors. Advanced Materials published by Wiley-VCH GmbH

15214095, 2024, 27, Downloaded from https://onlinelibrary.wiley.com/doi/10.1002/adma.202313125 by ALbert-Ludwigs-Universitaet, Wiley Online Library on [20/12/2024]. See the Terms and Conditions (https://onlinelibrary.wiley.com/terms-and-conditions) on Wiley Online Library for rules of use; OA articles are governed by the applicable Creative Commons License

15214095, 2024, 27, Downloaded from https://onlinelibrary.wiley.com/doi/10.1002/adma.202313125 by ALbert-Ludwigs-Universitaet, Wiley Online Library on [20/12/2024]. See the Terms and Conditions (https://onlinelibrary.wiley.com/terms-and-conditions) on Wiley Online Library for rules of use; OA articles are governed by the applicable Creative Commons License

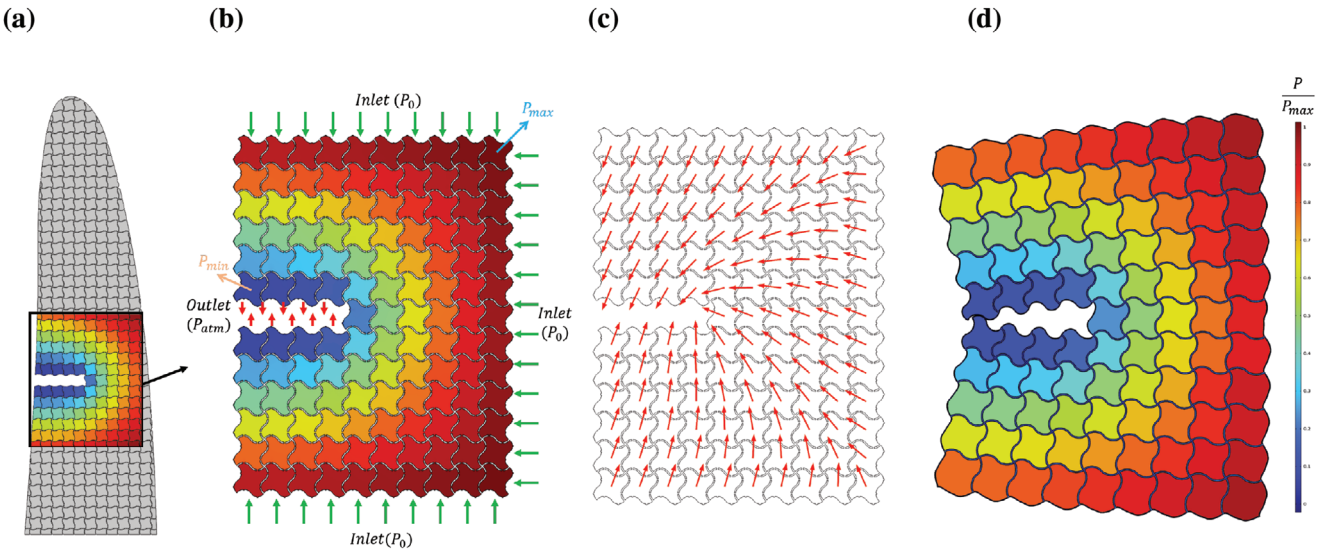


Figure 6. a) Damaged metamaterial mimicking the hydraulically driven self-sealing of the succulent *Delosperma cooperi* leaves, b) pressure gradient in the cracked area of the metamaterial, c) fluid flow toward the out of metamaterial due to the disturbance of mechanical equilibrium, d) crack closure by deformation of the metamaterial around due to pressure gradient (the colors of hydrostatic pressure gradient and deformed metamaterial were superimposed).

cracks of varying lengths. The parameter α was defined as the ratio of the crack length to the length of the metamaterial structure ($\alpha = \frac{L_{Crack}}{L_{Metamaterial}}$), indicating the severity of damage in the metamaterial. **Figures** 8a–e displays mechanical metamaterials consisting of unit cells with a normalized radius of $r/l = 0.26$ and a slenderness ratio of $t/l = 0.05$. The colormaps in Figures 8a to e, illustrate the pressure gradients resulting from different cracks with $\alpha = 56\%$, 45%, 34%, 23%, 12%. Based on the results shown in these figures,the greater the crack length (higher α), the larger the crack surface and fluid outlet, leading to a substantial low-pressure area around the damaged zone. Hence, the deformation of the metamaterial due to the corresponding pressure gradients, and the low-pressure zone creates the necessary volume change for $\alpha = 56\%$ and $\alpha = 45\%$ to completely close the crack (Figure 8a,e). However, crack closure was not successful for smaller crack lengths (Figure 8c, d, e). As discussed in the context of Figure 7, implementing lower values of normalized radius can improve the volume change necessary

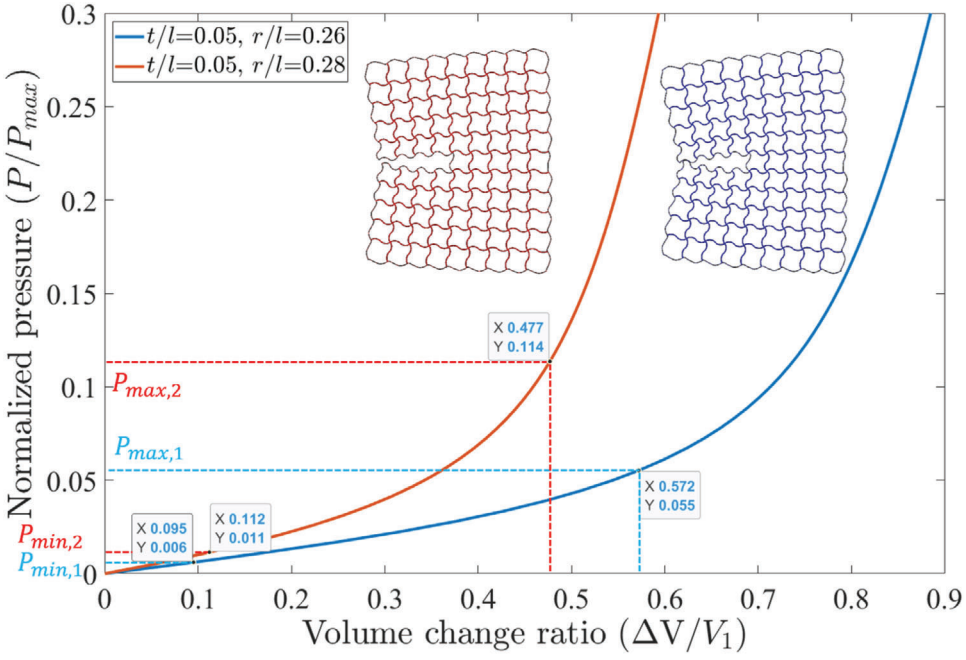


Figure 7. Crack closure behavior of two different metamaterials with $r/l = 0.26$ and $r/l = 0.28$.

© 2024 The Authors. Advanced Materials published by Wiley-VCH GmbH

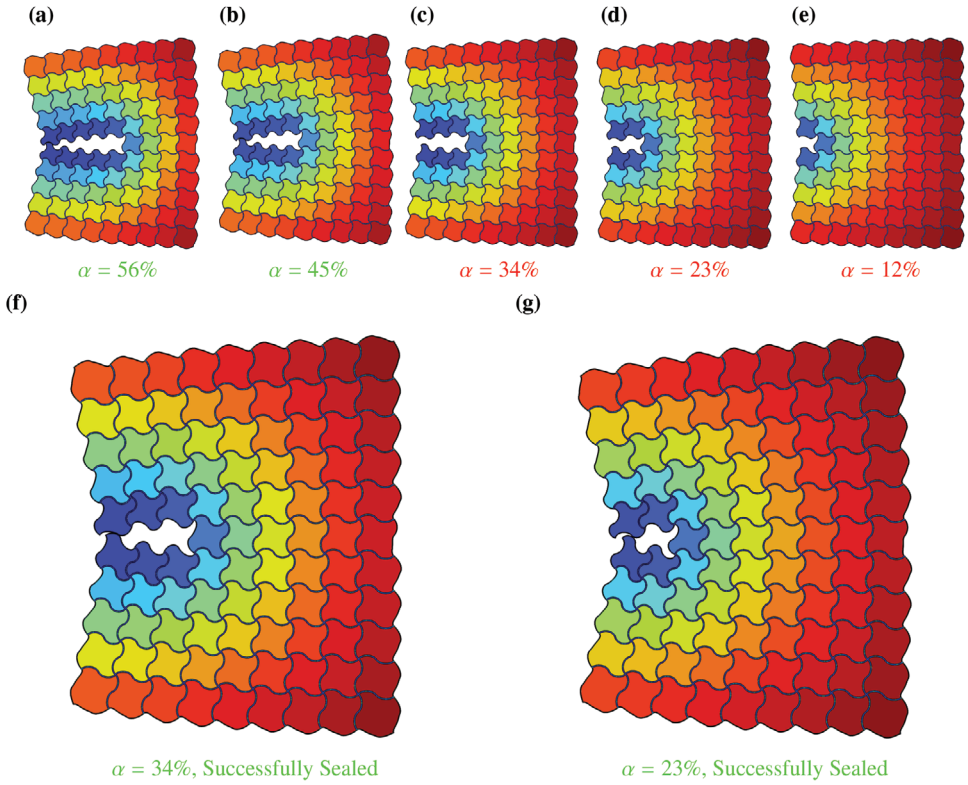


Figure 8. Self-sealing efficiency for various relative crack lengths α. a–e) Final sealed condition of the cracked metamaterials with $r/l = 0.26$ unit cells according to the distribution of internal pressure, f–g) successful sealing mechanism for metamaterials with crack length of $\alpha = 34\%$ and $\alpha = 23\%$ after implementing the $r/l = 0.25$ unit cells.

for the sealing mechanism. Figure 8f,g illustrates cracked metamaterials with a structure made of $r/l = 0.25$, which exhibits a higher volume change at the same pressure gradient (see Figure 4a). It is evident that these structures can successfully close the crack gap even for smaller crack lengths ($\alpha = 34\%$ and $\alpha = 23\%$).

It is worth highlighting that, in reality, the damage can be quite irregular, resulting in non-straight cracks. To address this issue, four cracks of different geometries are introduced to assess the self-sealing functionality of developed metamaterial. A metamaterial composed of unit cells with normalized radius of $r/l = 0.28$ and slenderness ratio of $t/l = 0.5$ is selected for this analysis. **Figure 9**a–d illustrates the horizontal crack with asymmetry, inclined crack with a 45-degree slope, zigzag-shaped crack, and an irregular crack, respectively. The cracks are introduced to the metamaterial by removing the irregular pattern of unit cells according to the assumed crack shapes. Since the shapes of the cracks are not regular and symmetrical, the resulting pressure gradient is noticeably non-homogeneous. Following the non-uniform distribution of fluid pressure in the metamaterials, non-homogeneous deformation patterns were observed in the unit cells around the cracked area. Despite the fact that the introduced cracks are relatively large in comparison to the metamaterial's total dimensions, the metamaterials showed significant global shape morphing required for closing the outlet gap and reducing the fluid flow to the outside of the metamaterial system (see Figure 9e–h).

When selecting manufacturing method, one should keep in mind that the designed metamaterial has to be deformable enough to carry the high strains from large deformations, initially sealed from the leakage under high hydrostatic pressures, but simultaneously facilitates the exchange of the fluid between unit cell. Here, the metamaterial satisfying these requirements was fabricated from soft silicone rubber using puzzle-like molds (see Section SC, Supporting Information for details of step-by-step manufacturing process). **Figure 10**a illustrates the experimental setup used to demonstrate the self-sealing deformation of an example structure under real conditions. For the convenience of the experimental demonstration, air was employed to pressurize the metamaterial. A lattice structure, measuring 10 by 13 of the designed unit cell with a normalized radius of $r/l = 0.30$ and a slenderness ratio of $t/l = 0.05$, was constructed from stretchable Ecoflex rubber silicone (Ecoflex 00-50) to achieve the capability of high strains due to internal pressure and corresponding volume change. A transverse crack was applied to the metamaterial by cutting four unit cells from the left edge of the structure (Figure 10b). To maintain symmetrical boundary conditions due to the repeated structure in the third dimension, the metamaterial was placed between two Plexiglases to keep the structure undeformed in the out-of-plane direction. Additionally, a low-viscosity lubricant was applied to reduce friction between the sample and the glasses. The fluid (i.e., air) was injected from a single inlet point on the opposite side of the cracked zone. To facilitate conditions closer resembling those used in simulations

© 2024 The Authors. Advanced Materials published by Wiley-VCH GmbH

15214095, 2024, 27, Downloaded from https://onlinelibrary.wiley.com/doi/10.1002/adma.202313125 by ALbert-Ludwigs-Universitaet, Wiley Online Library on [20/12/2024]. See the Terms and Conditions (https://onlinelibrary.wiley.com/terms-and-conditions) on Wiley Online Library for rules of use; OA articles are governed by the applicable Creative Commons License

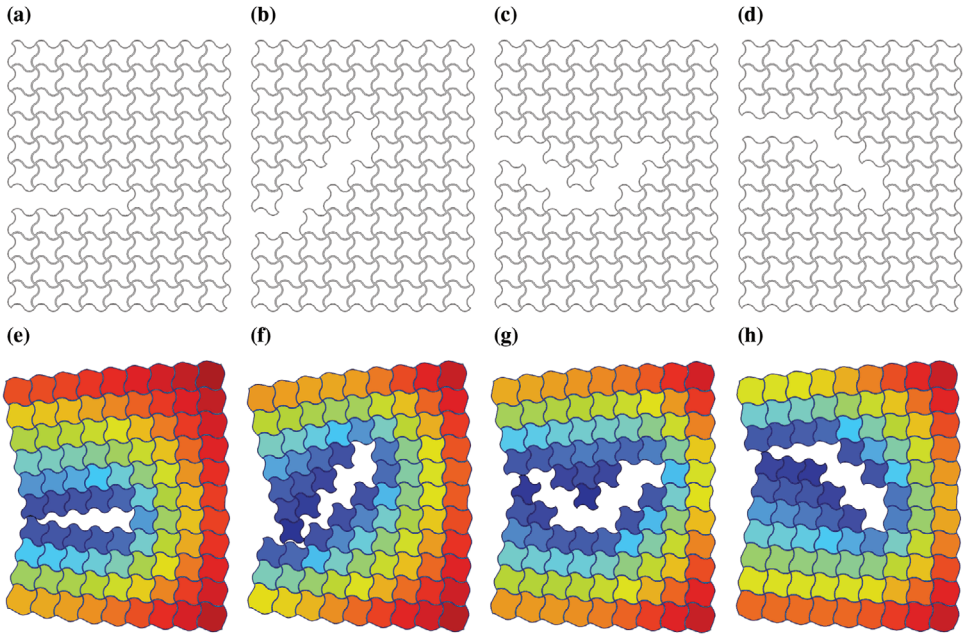


Figure 9. Self-sealing efficiency for various crack shapes. a–d) Different crack shapes with horizontal (asymmetrical), inclined, zigzag, and irregular cracks, e–h) effectively closed cracks by bringing the crack edges together and reduction of fluid flow.

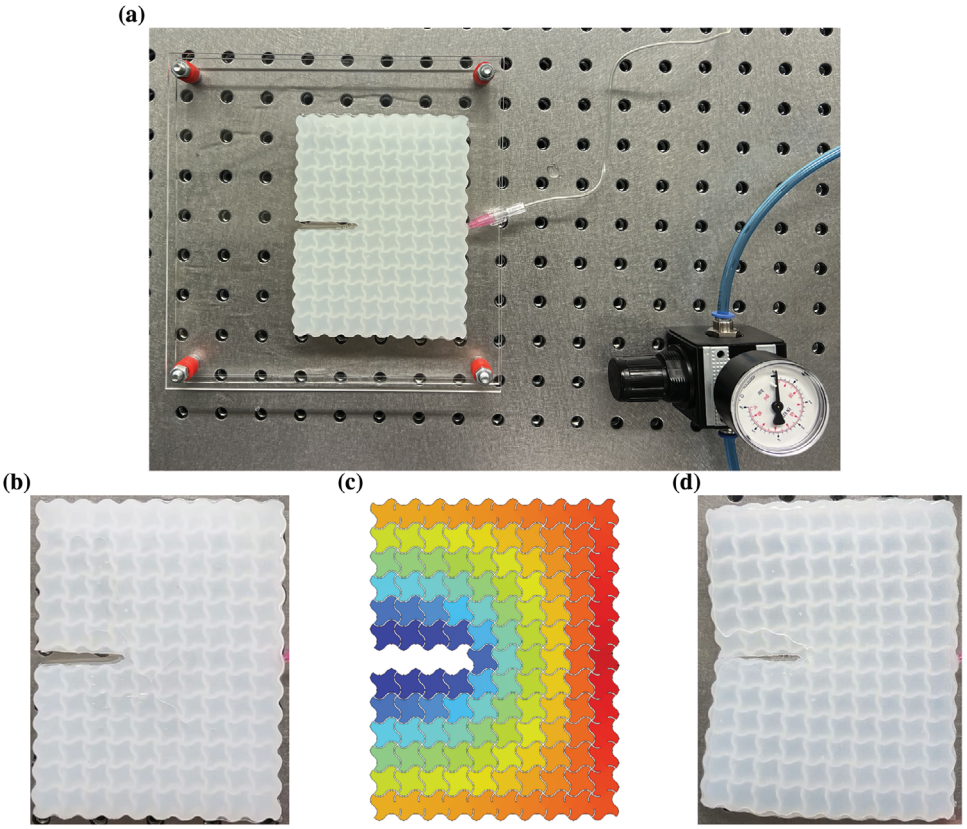


Figure 10. Crack closure of the self-sealing metamaterial consisting of unit cell with a normalized radius of $r/l = 0.30$ and a slenderness ratio of $t/l = 0.05$. a) Experimental set-up for applying the air pressure to the cracked metamaterial, b) initial shape of the metamaterial with $P_{in} = 0$, c) pressure gradient resulting from the local inlet, d) final shape of the metamaterial with $P_{in} = P_0$.

© 2024 The Authors. Advanced Materials published by Wiley-VCH GmbH

15214095, 2024, 27, Downloaded from https://onlinelibrary.wiley.com/doi/10.1002/adma.202313125 by ALbert-Ludwigs-Universitaet, Wiley Online Library on [20/12/2024]. See the Terms and Conditions (https://onlinelibrary.wiley.com/terms-and-conditions) on Wiley Online Library for rules of use; OA articles are governed by the applicable Creative Commons License

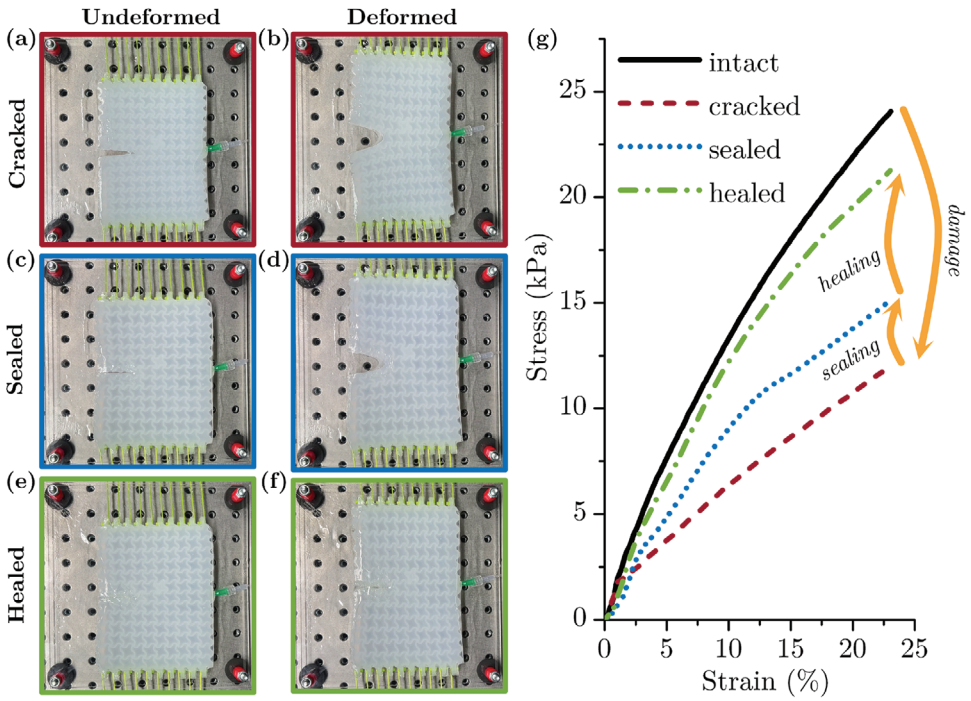


Figure 11. Undeformed and deformed states of the mechanical metamaterial under axial loading in (a, b) cracked, (c,d) sealed and (e, f) healed conditions, (g) stress-strain curves for mechanical metamaterial with $t/l = 0.05$ and $r/l = 0.26$, in the intact, cracked, sealed, and healed conditions.

and enable the pressurization with a single inlet, the higher permeability in the unit cells at the intact sides of the metamaterial was introduced by increasing the diameter of the holes between unit cells. This adjustment ensured that the pressure gradient within the lattice resembled the actual pressure gradient, as shown in Figure 10c, where the fluid starts to flow at the edges initially, acting as a distributed inlet for the lattice structure. As a final result, the metamaterial deformation followed the pressure gradient, successfully closing the crack (Figure 10d). Although the manufactured specimen was able to demonstrate the basic self-sealing ability similar to the observed in *Delosperma cooperi* plant, a slight difference in deformations between the experimental and simulation results was observed. The thin layer of silicone on two sides of the structure, designed to maintain the flow in the structure, and the friction between the symmetrical glasses could be considered the most dominant causes of the deviation in the final results. The straight thin walls significantly increased the stiffness of the structure, requiring high pressure (around 2 bar) to inflate the metamaterial.

As already mentioned, two core benefits of the self-sealing process in biological materials are decreasing the crack area and, more importantly, assisting in the subsequent self-healing process by bringing crack faces together. To prove that similar behavior can be observed in the proposed metamaterial concept, we performed additional experiments on fabricated specimens. Beyond the ability to pressurize and depressurize the considered metamaterial, we were able to assess its reaction to tensile loading using a custom-built testing setup. The details of the experimental setup and the designed grippers for applying the tensile loading to the specimen can be found in Section SC (Supporting Information). First, the intact specimen was subjected to a tensile load to have a reference stress-strain curve (solid black line in **Figure 11g**). A specimen without the crack experiences relatively uniform stretching with lateral shrinkage. If a crack is introduced on the side of the specimen, then the subsequent loading results in the noticeable opening of the crack tip (Figure 11a,b). The pressurizing of the metamaterial interior in an undeformed state leads to generating the pressure gradient, which yields the self-sealing and closure of the crack, in line with the simulation results (Figure 11c). Since the crack faces are not attached to each other, subsequent loading causes further crack opening. At the same time, due to the internal pressure gradient inside the metamaterial structure, it demonstrates a smaller crack tip angle (Figure 11d) as compared with the non-pressurized case (Figure 11b). Simultaneously, sealing results in a stiffer response of the metamaterials, as shown in Figure 11g. Therefore, even without a self-healing process taking place, the self-sealing helps to bring the crack faces together, reduce the crack opening angle and partially restore the stiffness of the metamaterial. To further highlight the importance of self-sealing for the subsequent realization of the self-healing process, we carefully applied a healing agent of Ecoflex 00-35 fast-cure silicone rubber on the faces of cracked specimens. This is a simplification of the process happening in the biological model, aimed purely at demonstrating the interplay between self-sealing and self-healing. About five minutes after application, the first specimen without internal pressure was subjected to stretching. Since the faces of the crack were never in contact (Figure 11a), the existence of the liquid silicone did not affect the deformation behavior of the specimen. In contrast, when internal pressure was added to the specimen, pushing the crack faces together, curing of the silicone led to the closure of the crack (Figure 11e). Subsequent

© 2024 The Authors. Advanced Materials published by Wiley-VCH GmbH

15214095, 2024, 27, Downloaded from https://onlinelibrary.wiley.com/doi/10.1002/adma.202313125 by ALbert-Ludwigs-Universitaet, Wiley Online Library on [20/12/2024]. See the Terms and Conditions (https://onlinelibrary.wiley.com/terms-and-conditions) on Wiley Online Library for rules of use; OA articles are governed by the applicable Creative Commons License

stretching demonstrates reliable attachment between crack faces and reveals noticeable stiffening of the specimen. Unsurprisingly, the healed specimen still underperforms compared to the intact one (Figure 11g). However, the stress-strain curves show a much stiffer response as compared with a damaged metamaterial. This fact emphasizes the importance of the sealing phase; without bringing the crack surfaces into contact, even with the presence of the healing agent, the healing phase cannot be completed, and the crack surfaces will stay separated.

3. Conclusion

In conclusion, programmable mechanical metamaterials offer an incredible design space that allows the integration of novel and advanced abilities into materials. Notably, their behavior is predominantly dictated by the fundamental unit cell structure, facilitating the accurate prediction of interactions with incoming signals. This contrasts with conventional materials design, making the attainment of metamaterial design significantly more accessible. A step-by-step programming of the basic unit cell structures within the mechanical metamaterial makes it possible to achieve the integration of complex functions and algorithms, similar to those found in living nature. In this study, we demonstrated that through a comprehensive analysis of self-sealing in the succulent leaves of *Delosperma cooperi*, the necessary properties and features of the interconnected cellular structure can be extracted and translated into mechanisms and functions available in mechanical metamaterials. It is noteworthy that the use of systematic approaches can greatly facilitate the transfer of knowledge from biological models to technical systems.[1,27,41] Transferring the essential characteristics of the plant tissue encoding the self-sealing ability is a crucial step toward creating damage-tolerant engineered materials. Here, the pressure-dependent volume change and permeability of the underlying cell structure, as well as the necessary information gradients about the local damage, allow a successful implementation of this ability into an artificial mechanical metamaterial. The parameter space provided by the slenderness ratio and radius of the curved shells within the unit cells allowed fine-tuning to reach the expected nonlinear mechanical behavior. The overall stiffness and transition point during expansion, together with the permeability, can be adapted to accommodate various crack sizes as well as tune the reaction time. Nevertheless, while the design space of programmable materials invites creativity, the manufacturing process becomes the real challenge. The unit cell design presented here requires precise structural manufacturing, as bending stiffness or fluid flow through holes is highly nonlinear in nature. In this regard, the fabrication of the hollow and permeable structures was made possible by a single-shot mold and successfully produced a perfectly sealed and inflatable metamaterial. Moreover, this modular manufacturing method can easily be scaled up. Finally, having a mechanical metamaterial that can seal cracks independently of the surrounding environment brings us one step closer to materials with a self-repairing ability. This opens up a new research challenges to combine structural or mesoscopic self-sealing mechanisms similar to the proposed mechanical metamaterial in this study, with available self-healing methods such as light- or heat-induced healing polymers,[42] capsule-based systems,[43] or vascular-network healing techniques,[44] to complete the repairing process and fully restore the functionality and mechanical properties of the material system even after enduring large or repeated damage.

Supporting Information

Supporting Information is available from the Wiley Online Library or from the author.

Acknowledgements

This work was funded by the Deutsche Forschungsgemeinschaft (DFG, German Research Foundation) under Germany's Excellence Strategy – EXC-2193/1 – 390951807. C.E. acknowledged partial funding provided by the Fraunhofer Cluster of Excellence Programmable Materials. The authors thank Lina Manuela Rojas for the great assistance in manufacturing of the experimental prototypes.

Open access funding enabled and organized by Projekt DEAL.

Conflict of Interest

The authors declare no conflict of interest.

Author Contributions

Naeim Ghavidelnia performed conceptualization, writing, original draft, visualization, finite element simulations and experiments; Olga Speck performed supervision, writing, review, and editing of the manuscript; Viacheslav Slesarenko performed supervision, writing, review, and editing of the manuscript; Christoph Eberl performed conceptualization, funding acquisition, and supervision.

Data Availability Statement

The data that support the findings of this study are available from the corresponding author upon reasonable request.

Keywords

bio-inspired, *Delosperma cooperi*, mechanical metamaterials, programmable materials, self-sealing

Received: December 4, 2023
Revised: April 4, 2024
Published online: April 30, 2024

[1] O. Speck, T. Speck, *Biomimetics* **2019**, *4*, 26.
[2] V. C. Li, A. R. Sakulich, H. W. Reinhardt, E. Schlangen, K. van Tittelboom, D. Snoeck, N. De Belie, C. Joseph, D. R. Gardner, R. J. Lark, H. Mihashi, T. Nishiwaki, *Self-Healing Phenomena in Cement-Based Materials. RILEM State-of-the-Art Reports* (Eds: M. de Rooij, K. van Tittelboom, N. de Belie, E. Schlangen), vol. *11*, Springer, Dordrecht **2013**, pp. 119–215.
[3] S. K. Ghosh, *Self-Healing Materials: Fundamentals, Design Strategies, and Applications*, vol. *18*, Wiley Online Library, Weinheim **2009**.
[4] R. P. Wool, *Soft Matter* **2008**, *4*, 400.
[5] M. D. Hager, P. Greil, C. Leyens, S. van der Zwaag, U. S. Schubert, *Adv. Mater.* **2010**, *22*, 5424.

© 2024 The Authors. Advanced Materials published by Wiley-VCH GmbH

15214095, 2024, 27, Downloaded from https://onlinelibrary.wiley.com/doi/10.1002/adma.202313125 by ALbert-Ludwigs-Universitaet, Wiley Online Library on [20/12/2024]. See the Terms and Conditions (https://onlinelibrary.wiley.com/terms-and-conditions) on Wiley Online Library for rules of use; OA articles are governed by the applicable Creative Commons License

[6] S. R. White, N. R. Sottos, P. H. Geubelle, J. S. Moore, M. R. Kessler, S. Sriram, E. N. Brown, S. Viswanathan, *Nature* **2001**, *409*, 794.
[7] S. R. White, B. J. Blaiszik, S. L. Kramer, S. C. Olugebefola, J. S. Moore, N. R. Sottos, *Am. Sci.* **2011**, *99*, 392.
[8] M. Alshaaer, S. A. Mallouh, J. Al-Kafawein, Y. Al-Faiyz, T. Fahmy, A. Kallel, F. Rocha, *Appl. Clay Sci.* **2017**, *143*, 125.
[9] M.-L. Song, H.-Y. Yu, L.-M. Chen, J.-Y. Zhu, Y.-Y. Wang, J.-M. Yao, Z. Zou, K. C. Tam, *ACS Sustainable Chem. Eng.* **2019**, *7*, 6969.
[10] M. Ali, A. Abu-Tair, J. Kinuthia, R. Babecki, *Build. Res. Inf* **2015**, *43*, 253.
[11] S. Wang, M. W. Urban, *Nat. Rev. Mater.* **2020**, *5*, 562.
[12] S. Zhang, N. van Dijk, S. van der Zwaag, *Acta Metall. Sin. (Engl. Lett.)*. **2020**, *33*, 1167.
[13] F. Li, H.-Y. Yu, Y.-Y. Wang, Y. Zhou, H. Zhang, J.-M. Yao, S. Y. H. Abdalkarim, K. C. Tam, *J. Agric. Food Chem.* **2019**, *67*, 10954.
[14] A. Azizi, M. R. Gadinski, Q. Li, M. A. AlSaud, J. Wang, Y. Wang, B. Wang, F. Liu, L.-Q. Chen, N. Alem, Q. Wang, *Adv. Mater.* **2017**, *29*, 1701864.
[15] F. An, X. Li, P. Min, H. Li, Z. Dai, Z.-Z. Yu, *Carbon* **2018**, *126*, 119.
[16] M. A. Mohammadi, R. Eslami-Farsani, H. Ebrahimnezhad-Khaljiri, *Polym. Test.* **2020**, *91*, 106862.
[17] P. Greil, *Adv. Eng. Mater.* **2020**, *22*, 1901121.
[18] P. Greil, *J. Adv. Ceram.* **2012**, *1*, 249.
[19] V. K. Mohonee, K. L. Goh, L. Mishnaevsky Jr, P. Pasbakhsh, *Comput. Mater. Sci.* **2021**, *192*, 110203.
[20] K. Van Tittelboom, N. De Belie, *Materials* **2013**, *6*, 2182.
[21] M. Wu, B. Johannesson, M. Geiker, *Constr. Build. Mater.* **2012**, *28*, 571.
[22] J. Wang, Q. Gao, F. Zhao, J. Ju, *Crit. Rev. Food Sci. Nutr.* **2023**, 1, https://doi.org/10.1080/10408398.2023.2232877.
[23] J. Yang, Z. Sun, N. De Belie, D. Snoeck, *Cem. Concr. Res.* **2023**, *170*, 107183.
[24] C. Zhang, R. Liu, M. Chen, X. Li, Z. Zhu, J. Yan, *Constr. Build. Mater.* **2022**, *347*, 128626.
[25] H. Lee, H. Wong, N. Buenfeld, *Cem. Concr. Res.* **2016**, *79*, 194.
[26] T. Speck, R. Mülhaupt, O. Speck, *Self-Healing Polymers: From Principles to Applications*, Wiley Online Library, Weinheim **2013**, pp. 61–89.
[27] ISO:18458, Biomimetics—Terminology, concepts and methodology, Standard ISO 18458:2015, International Organization for Standardization, **2021**.
[28] S. Busch, R. Seidel, O. Speck, T. Speck, *Proc. R. Soc. B: Biol. Sci.* **2010**, *277*, 2113.
[29] O. Speck, M. Schlechtendahl, F. Borm, T. Kampowski, T. Speck, *Beilstein J. Nanotechnol.* **2018**, *9*, 175.
[30] H. Klein, L. Hesse, M. Boljen, T. Kampowski, I. Butschek, T. Speck, O. Speck, *J. Theor. Biol.* **2018**, *458*, 184.
[31] J. Dumais, Y. Forterre, *Annu. Rev. Fluid Mech.* **2012**, *44*, 453.
[32] W. Konrad, F. Flues, F. Schmich, T. Speck, O. Speck, *J. Theor. Biol.* **2013**, *336*, 96.
[33] Y. Yang, D. Davydovich, C. C. Hornat, X. Liu, M. W. Urban, *Chem* **2018**, *4*, 1928.
[34] J. Becker, O. Speck, T. Göppert, T. Speck, C. Müller, *Adv. Intell. Syst.* **2022**, *4*, 2200215.
[35] A. A. Zadpoor, *Mater. Horiz.* **2016**, *3*, 371.
[36] J.-H. Lee, J. P. Singer, E. L. Thomas, *Adv. Mater.* **2012**, *24*, 4782.
[37] G. Felsch, N. Ghavidelnia, D. Schwarz, V. Slesarenko, *Comput. Methods Appl. Mech. Eng.* **2023**, *410*, 116032.
[38] K. Bertoldi, V. Vitelli, J. Christensen, M. Van Hecke, *Nat. Rev. Mater.* **2017**, *2*, 1.
[39] N. Ghavidelnia, K. Yin, B. Cao, C. Eberl, *Mater. Des.* **2023**, *230*, 111988.
[40] D. Schwarz, G. Felsch, F. Tauber, S. Schiller, V. Slesarenko, *Mater. Des.* **2023**, 112468.
[41] B. Cao, N. Ghavidelnia, O. Speck, C. Eberl, *Program. Mater.* **2023**, *1*, e12.
[42] C.-M. Chung, Y.-S. Roh, S.-Y. Cho, J.-G. Kim, *Chem. Mater.* **2004**, *16*, 3982.
[43] P. C. JE, M. T. Sultan, C. P. Selvan, S. Irulappasamy, F. Mustapha, A. A. Basri, S. N. Safri, *J. Mater. Res. Technol.* **2020**, *9*, 7370.
[44] B. J. Blaiszik, S. L. Kramer, S. C. Olugebefola, J. S. Moore, N. R. Sottos, S. R. White, *Annu. Rev. Mater. Res.* **2010**, *40*, 179.

© 2024 The Authors. Advanced Materials published by Wiley-VCH GmbH

15214095, 2024, 27, Downloaded from https://onlinelibrary.wiley.com/doi/10.1002/adma.202313125 by ALbert-Ludwigs-Universitaet, Wiley Online Library on [20/12/2024]. See the Terms and Conditions (https://onlinelibrary.wiley.com/terms-and-conditions) on Wiley Online Library for rules of use; OA articles are governed by the applicable Creative Commons License